Journal of Photochemistry & Photobiology A: Chemistry 372 (2019) 89–98

Contents lists available at ScienceDirect

Journal of Photochemistry & Photobiology A: Chemistry

journal homepage: www.elsevier.com/locate/jphotochem

Ultrafast excited state dynamics of a stilbene–viologen charge transfer complex and its interaction with alkanediammonium salts

Mikhail V. Rusalov[a,*], Valery V. Volchkov[a], Vladimir L. Ivanov[a], Mikhail Ya. Melnikov[a], Fedor E. Gostev[b], Victor A. Nadtochenko[a,b], Artem I. Vedernikov[c], Sergey P. Gromov[a,c], Michael V. Alfimov[c]

[a] Chemistry Department, M.V. Lomonosov Moscow State University, Leninskie Gory 1-3, Moscow, 119991, Russian Federation
[b] N.N. Semenov Institute of Chemical Physics, Russian Academy of Sciences, Kosygina Str. 4, Moscow, 119991, Russian Federation
[c] Photochemistry Center, Federal Scientific Research Center "Crystallography and Photonics", Russian Academy of Sciences, Novatorov Str. 7A-1, Moscow, 119421, Russian Federation

ARTICLE INFO

Keywords:
Bis-crown ether
Transient absorption spectroscopy
Ultrafast electron transfer
Charge transfer complex
Fluorescence

ABSTRACT

The spectral and thermodynamic properties of charge transfer complexes **D·A** and **D·A·D** between (*E*)-bis(18-crown-6) stilbene (**D**) and 1,1′-bis(2-ammonioethyl)-4,4′-bipyridinium tetraperchlorate (**A**) in MeCN were studied. The complex **D·A** is highly stable, while the complex **D·A·D** is weakly stable. **D·A** does not fluoresce due to fast intramolecular processes of direct and reverse electron transfer. The efficiency of **D·A** fluorescence ignition upon adding alkanediammonium salts depends on the length of a carbon chain. The spectral and kinetic characteristics of **D·A** and **D·A·D** CT states were obtained by femtosecond transient absorption spectroscopy. It was established that the characteristic time of back electron transfer in the CT state of **D·A·D** (770 fs) is significantly higher than that in the CT state of **D·A** (400 fs). In a number of charge transfer complexes, formed by derivatives of 4,4′-bipyridinium and di-(4-pyridinium)-ethylene with ammonioethyl and ammoniopropyl *N*-substituents, the rate of back electron transfer depends weakly on the acceptor nature, but is determined by the length of the carbon chain of terminal groups.

1. Introduction

Organic diamines play an important role in polymer chemistry and technology [1], in biochemistry, pharmacology, and medical diagnostics [2]. Therefore, the problem of development of molecular sensors for qualitative and quantitative determination of diamines and their salts in natural, industrial and biological samples attracts wide interest [3]. Bitopic molecular optical sensors were described in literature, which are based on crown-ethers [4–6], calixarenes [7], cucurbiturils [8]. They are capable of binding firmly and selectively diammomium ions into pseudocyclic complexes due to the formation of multiple hydrogen bonds. A more fine tuning of the sensors to certain, including natural, substrates is possible by involving in their structure such fragments that are capable of additional intermolecular interactions: stacking, hydrophobic and van der Waals. Crown-containing porphyrins [9] and cyclodextrins [10,11] can served as examples of such compounds.

Supramolecular charge transfer complexes (CTC), formed by chromogenic bis-crown ethers and viologen analogues with terminal ammonioalkyl groups, are referred as promising optical molecular sensors for determination of organic and inorganic cations [12–23]. Together with the host-guest interaction between macrocyclic moieties and ammonioalkyl groups, there is also a donor-acceptor interaction between aromatic systems of a donor and an acceptor. Due to this fact, the organic supramolecular CTCs possess a number of characteristic properties: redox potentials of a donor and an acceptor undergo significant shifts [14]; the complexes can be colored due to light absorption at the CT band; they do not fluoresce practically because of ultrafast processes of direct and back electron transfer, which compete successfully with the radiative deactivation process [17,20,23].

The competitive binding of metal cations or diammonium ions leads to the suppression of intramolecular electron transfer processes and to the ignition of solvent fluorescence. That is why supramolecular CTCs are considered to be promising molecular sensors for the determination of organic [13] or inorganic [18,20–23] cations.

Due to high thermodynamic stability and ease of self-assembling process, supramolecular CTCs are convenient objects for studying of ultrafast photoinduced electron transfer [17,22,23]. The structure of supramolecular CTCs makes it possible to vary effectively the chemical nature of a donor and an acceptor, as well as their mutual geometric arrangement.

* Corresponding author.
E-mail address: mvrusalov@yandex.ru (M.V. Rusalov).

https://doi.org/10.1016/j.jphotochem.2018.12.007
Received 8 July 2018; Received in revised form 29 November 2018; Accepted 5 December 2018
Available online 06 December 2018
1010-6030/

The ultrafast intramolecular electron transfer has been the subject of intensive study for last two decades [24]. The intramolecular character of this process allows us to exclude the effects of translational diffusion and chaotic orientation of reagents, taking place upon intermolecular electron transfer. This gives an opportunity to compare directly the experimental data with predictions of different theoretical models. In the solvents with small relaxation times (acetone, acetonitrile), the characteristic time of electron transfer is comparable with the solvent relaxation time and is controlled by the solvation process. In the solvents with big relaxation time (alcohols, glycols, esters), the characteristic time of electron transfer is significantly shorter than the relaxation time of the solvent.

The dependency of the reaction rate of back electron transfer on its driving force ($-\Delta G$) was the subject of detailed studies. The full bell-shaped relationship between the reaction rate of electron transfer and its driving force had already been demonstrated. This, according to Marcus semiclassical theory [25], corresponds to three modes of the reaction: normal, barrierless, and inverted [26,27].

In a number of cases, instead of the quadratic relationship between the logarithm of rate constant and a value of $-\Delta G$, a decreasing linear dependence was observed [28,29]. This can be connected with a gradual change of electron structure and geometry of ion-radical pairs as the difference of donor and acceptor electrochemical potentials grows [30]. The rate of electron transfer can demonstrate a well-marked viscosity dependence for covalent bonded donor-acceptor systems, including those by polymethylene bridges [31–33]. This can accounted for by the fact that intramolecular processes of charge separation and recombination can result in mutual rotation of donor and acceptor moieties and in changing of the distance between them.

Hydrogen bond plays the most important role among all varieties of intermolecular interactions because of its orientation and high energy. The supramolecular systems with multiple hydrogen bonds have heightened thermodynamic stability [34]. However, electron transfer in such systems is insufficiently studied.

Previously we have studied the ultrafast electron transfer in supramolecular CTCs between (*E*)-bis(18-crown-6)stilbene (**D**) and dipyridylethelene derivatives. 4,4′-(*E*)-ethene-1,2-diylbis[1-(2-ammonioethyl) pyridinium] tetraperchlorate (**A2**) [22] and 4,4′-(*E*)-ethene-1,2-diylbis[1-(2-ammoniopropyl)pyridinium] tetraperchlorate (**A3**) [17] played the role of an electron acceptor, forming complexes **D·A2** and **D·A3** with the electron donor **D**, respectively. Using femtosecond transient absorption spectroscopy, it was found that the characteristic time of back electron transfer in acetonitrile (MeCN) is equal to 410 fs for **D·A2** and 540 fs for **D·A3**. A slower electron transfer in the last case was explained by a greater averaged interplane distance between the molecules of the donor and the accector because of longer side ammonioalkyl *N*-substituents. An increase in the interplane distance leads to the decrease of electron coupling matrix element from 0.13 eV to 0.10 eV, which, according to the Marcus theory, leads to a lower reaction rate constant [22].

In the present work we studied the femtosecond dynamics of excited states of the complexes 1:1 (**D·A**) and 2:1 (**D·A·D**) between bis(crown) stilbene **D** and 1,1′-bis(2-ammonioethyl)-4,4′-bipyridinium tetraperchlorate (**A**) in MeCN. Viologen **A** is a stronger electron acceptor, whose first reduction potential exceeds by 0.1 V the similar value the acceptors **A2** and **A3**, studied earlier [21]. The novelty of the present work as compared to our previous works [17,22,23] is as follows:

1) the decomposition of the donor-acceptor **D·A** complex under the influence of diammonium ions was studied. Previously, we investigated the decomposition of the **D·A2** complex at the presents of alkaline and alkaline-earth metal cations, which leads to fluorescence "switching-on" [22,23]. It was established that the activity of alkaline metal cations is considerably lower than that of alkaline-earth metal cations, the latter being characterized by higher density of electric charge. However, the binding of metal cations except of the most large-sized ones, is not a specific feature of bis-crown ethers. That is why it was of interest to study the decomposition of donor-acceptor complexes under the influence of diammonium ions, because their strong binding is a specific property of bis-crown ethers due to geometrical correspondence and the formation of stable pseudocyclic complexes;
2) the dynamics of back electron transfer depending on wavelength of exciting light was studied. The consideration of photoinduced electron transfer in **D·A** enabled us to study the effects of excited light wavelength on this process. Due to a shortwave shift of the absorption spectrum of **A** relative to the spectrum of **D**, the possibility arose of selective excitation of donor or acceptor subsystems;
3) The effects of Gibbs free energy changes on back electron transfer rate were studied. The investigation of electron transfer dynamics in **D·A** and **D·A1** in addition to earlier studied complexes **D·A2** and **D·A3** permitted us to verify the applicability of the semi-classical single-mode nonadiabatic theory for describing of electron transfer kinetics depending on the variation of Gibbs free energy changes and donor-acceptor interplane distance.

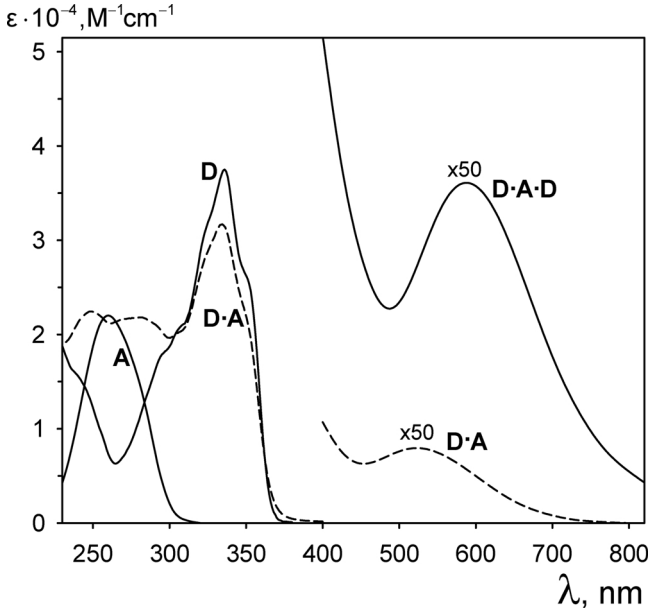

Fig. 1. Absorption spectra of **D**, **A**, **D·A** and **D·A·D** in MeCN. The CT band intensity of **D·A** and **D·A·D** is amplified 50 times.

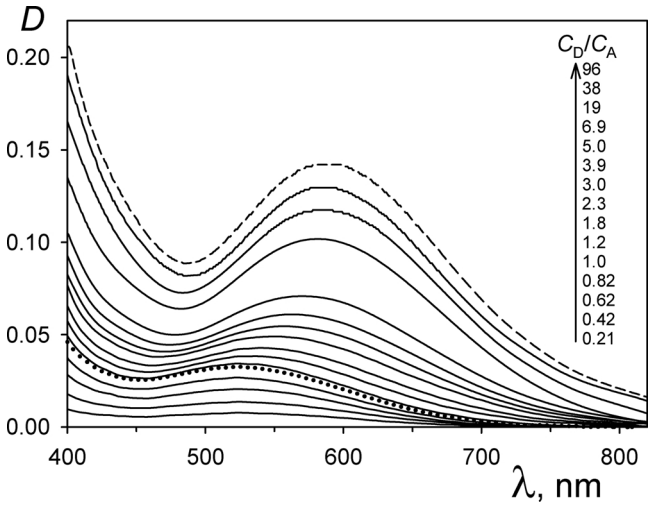

Fig. 2. The dependence of absorption spectra of the MeCN solution containing **A** (C = 0.2 mM) on the relative concentration of **D** (C_D/C_A varies from 0.21 to 96). The dotted line represents the spectrum when C_D/C_A is equal to unity. The dash line shows the calculated spectrum of the pure complex **D·A·D**.

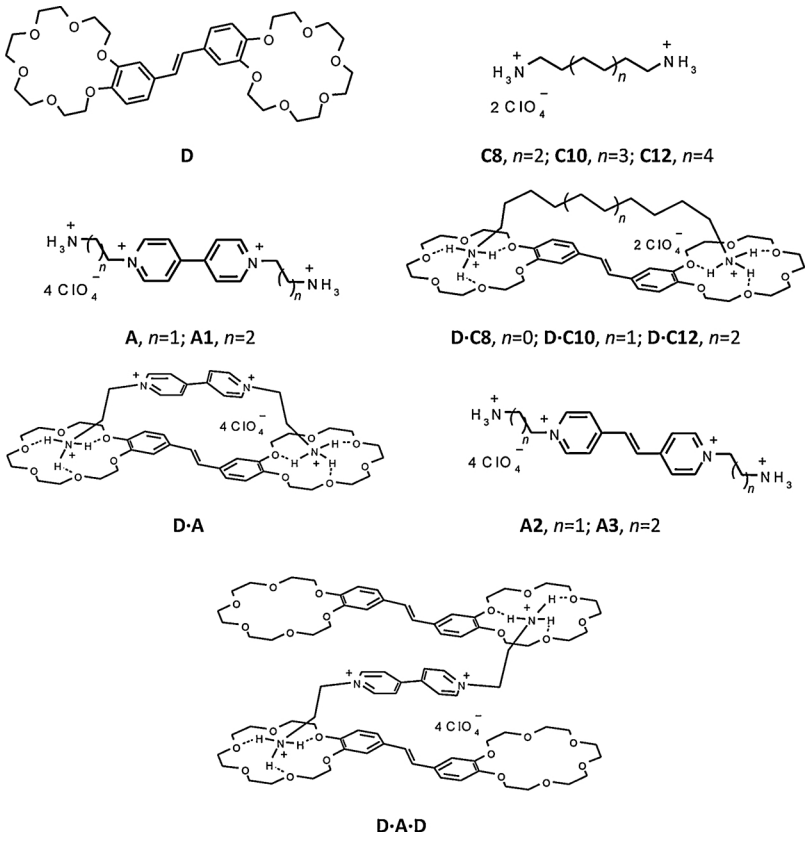

2. Results and discussion

2.1. Steady-state spectroscopy

Fig. 1 shows the absorption spectra of **D**, **A**, **D·A** and **D·A·D** in MeCN. The presence of wide weak bands in these spectra at 500–700 nm allows us to refer **D·A** and **D·A·D** to charge transfer complexes. Only the CT-band of **D·A·D** absorption spectrum is shown. The UV-part of the spectrum is absent because a great excess of **D** is needed for obtaining **D·A·D** complex in the solution.

The interaction of bis-crown ether **D** with viologen **A** leads to sequential formation of the complexes 1:1 (**D·A**) and 2:1 (**D·A·D**).

$$D + A \overset{K_1}{\rightleftarrows} D{\cdot}A \quad (1)$$

$$D{\cdot} + A + D \overset{K_2}{\rightleftarrows} D{\cdot}A{\cdot}D \quad (2)$$

Fig. 2 shows changes at long-wave band of the absorption spectrum **A** as **D** is added. When the relative donor concentration C_D/C_A is less than a unity, a monotonous growth of the absorption band with 524 nm maximum is observed. This indicates a formation of **D·A** according to Eq. (1). A further increase in **D** concentration leads to a bathochromic shift and to a significant increase of the intensity of long-wave absorption band. This is explained by the displacement of equilibrium towards the formation of **D·A·D** with the maximum 588 nm according to Eq. (2). As is seen from Fig. 2, a great excess of **D** concentration is required for comparatively complete binding of **A** into **D·A·D**, which points to weak stability of **D·A·D**. The **D·A·D** stability constant log K_2 is equal to 2.71, which was determined by spectrophotometric titration. The constant obtained is close to that of the 1:2 complex, which is formed by compound 1-(3-ammoniopropyl)-4-methylpyridinium diperchlorate with a single ammonioalkyl group (2.91) [18]. This indicates that each donor molecule of **D·A·D** is bound with the acceptor molecule through a single terminal group. In addition to absorption spectroscopy, the **D·A** formation was proven by ^{1}H-NMR spectroscopy, volt-amperometry and X-ray structural analysis [21]. The formation of 2:1 complexes similar to **D·A·D** was proven by Raman spectroscopy [15] and X-ray structural analysis [19].

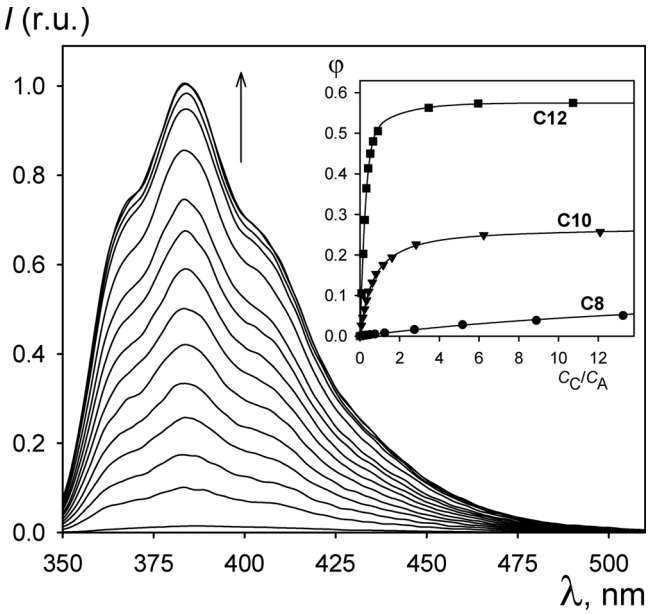

Fig. 3. Fluorescence enhancement of the MeCN solution containing **D** (C = 10 μM) and **A** (C = 30 μM) as a result of **C10** concentration increasing. Excitation wavelength is 330 nm. *Inset:* the dependence of fluorescence quantum yield (ϕ) on the relative concentration of a competitor (C_C/C_A). The solid line shows theoretically predicted trend obtained by using Eq. (3).

Table 1
The values of stability (K) and substitution (K_s) constants, absorption (λ_{abs}) and fluorescence (λ_{fl}) spectrum maxima, molar extinction coefficient (ε) and fluorescence quantum yield (ϕ) of **A**, **D**, and its complexes in MeCN.

	log K, M^{-1}	log K_s	λ_{abs}, nm	ε, M^{-1} cm^{-1}	λ_{fl}, nm	ϕ
A			260	22000	358	0.022
D			336	37500	386	0.39
D·C8	5.83 [13]	−1.63	335	34800	383.5	0.18
D·C10	7.58 [13]	0.24	334	36900	383	0.27
D·C12	8.59 [13]	1.07	333.5	38800	381	0.58
D·A	7.44		524	160		
			334	31700		
D·A·D	2.71		588	720		

In order to determine **D·A** stability constant, we used competitive spectrofluorometric titration. At the triple excess of **A**, the fluorescence of **D** is almost completely quenched because of practically complete displacement of equilibrium towards the formation of **D·A**, which does not fluoresce. The addition of alkanediammonium perchlorates (**C**) is accompanied by "switching-on" of donor fluorescence (Fig. 3). This can be explained by competitive binding of **D** by **C**, which leads to the formation of well-fluorescing complex **D·C** and to the elimination of **A** into the bulk according Eq. (3).

$$D\cdot A + C \overset{K_S}{\rightleftarrows} D\cdot C + A \tag{3}$$

The stability constant K_1 of **D·A** can be determined from Eq. (4), by using the substitution constant K_S and the stability constant K_C of **D·C**.

$$\log K_1 = \log K_C - \log K_S \tag{4}$$

As is seen from Fig. 3 (*Inset*), the efficiency of fluorescence ignition of **D·A** solution, when alkanediammonium salts are added, significantly depends on the length of a carbon chain, binding nitrogen atoms. This is caused by the dropping of affinity for **D** in a number of salts **C12**, **C10** and **C8**, as well as by the dropping of fluorescence quantum yield in a number of complexes **D·C12**, **D·C10** and **D·C8** (Table 1). Due to the fact that the length of **C8** carbon chain is too short for efficient binding of bis-crown ether **D**, even five-fold excess of **C8** leads only to a small growth of **D·A** solution fluorescence. From measurements with salts **C8**, **C10** and **C12**, the average value log K_1 is equal to 7.44 ± 0.09. The obtained stability constant of **D·A** is two orders of magnitude lower than those for **D·A2** and **D·A3** [17,22]. As in the case of alkanediammonium salts, this is due to a decrease in the internuclear distance between ammonium nitrogen atoms, at which the efficiency of their simultaneous binding by bis-crown ether decreases.

2.2. Transient absorption spectroscopy

In order to describe the evolution of transient absorption spectra, the multi-exponential function (5) was used.

$$\Delta D(\lambda,t) = A_0(\lambda) + \sum_{i=1}^{n} A_i(\lambda)\exp\left(-\frac{t}{\tau_i}\right) \tag{5}$$

Here, $\Delta D(\lambda, t)$ is a differential optical density matrix, which depends on time t and wavelength λ; $A_0(\lambda)$ is a background vector, which does not depend on time, n is a number of exponents; $A_i(\lambda)$ is a vector of pre-exponential factors of the i–th exponent, which depends on wavelength; τ_i is a characteristic time of i–th exponent. The characteristic times were found by the nonlinear least squares method, whereas the vectors of pre-exponential factors and the background vector were found by the linear least squares method. In practice, $A_i(\lambda)$ are often called as Decay Associated Spectra (DAS), while $A_0(\lambda)$ can be called as remaining spectrum if it changes in a wider time scale.

Fig. 4 (*Above*) shows the dynamics of transient absorption spectra of **D** (C = 0.5 mM) during the first 750 fs after the excitation by 330 nm 30 fs laser pulse. Spectral changes are satisfactorily described by Eq. (5)

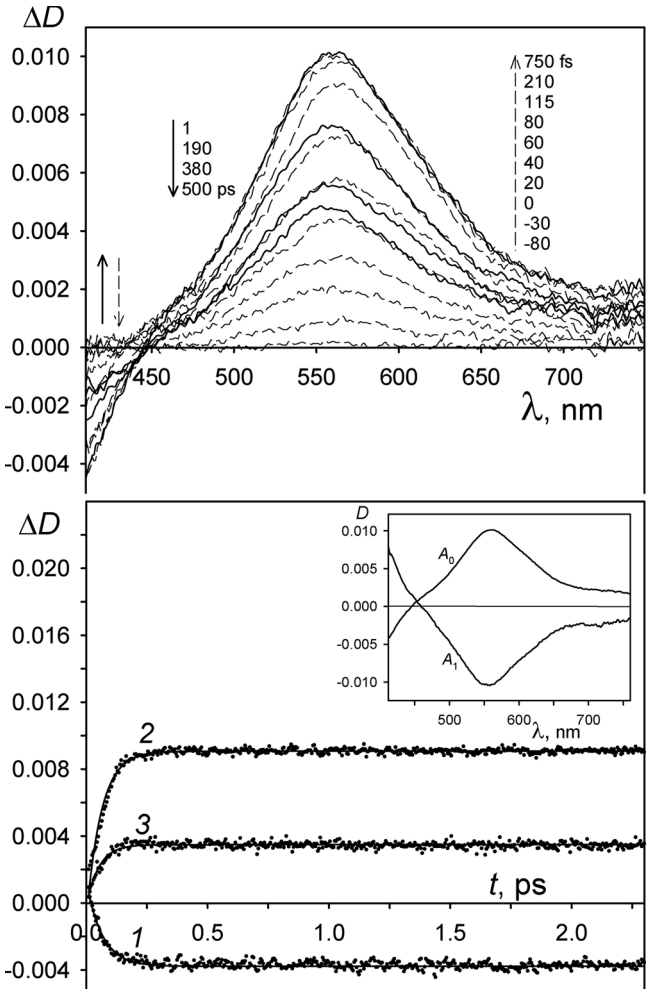

Fig. 4. *Above:* The dynamics of transient absorption spectra of **D** (C = 0.5 mM), which correspond to −80 to 750 fs delays (dash lines) and to 1 to 500 ps delays (solid lines), after the excitation by 330 nm 30 fs laser pulse. *Below:* The kinetic curves of transient absorption spectra for several wavelengths: (*1*) 415 nm, (*2*) 540 nm, (*3*) 650 nm. The solid lines represent fitting by mono-exponential function with characteristic time 60 fs. *Inset:* DAS correspond to characteristic times: (A_0) remaining spectrum, (A_1) 60 fs.

Table 2
Characteristic time (τ) and absolute maximum (λ_{abs}) of pre-exponential factors of femtosecond kinetics, obtained by excitation with a laser pulse of a certain wavelength (λ_{ex}).

Subst.	λ_{ex}, nm	Comp.	τ, fs	λ_{abs}, nm
D	330	**Ia**	60	557
A	260	**IIa**	140	407, 648
		IIb	1950	401, 602
D·A	330	**IIIa**	50	574
		IIIb	270	400, 522
		IIIc	400	399, 523
D·A	260	**IVa**	140	416, 601
		IVb	250	400, 522
		IVc	400	400, 522
D·A + D·A·D	330	**Va**	50	567
		Vb	270	532
		Vc	390	533
		Vd	770	578

under the assumption of mono-exponential law with the characteristic time 60 fs (**Ia**) (Fig. 4, *Below*). The *Inset* to Fig. 4 shows the spectral contributions of **Ia** (A_1) and remaining spectrum (A_0). During the first 200 fs, the growth of differential absorption as well as stimulated

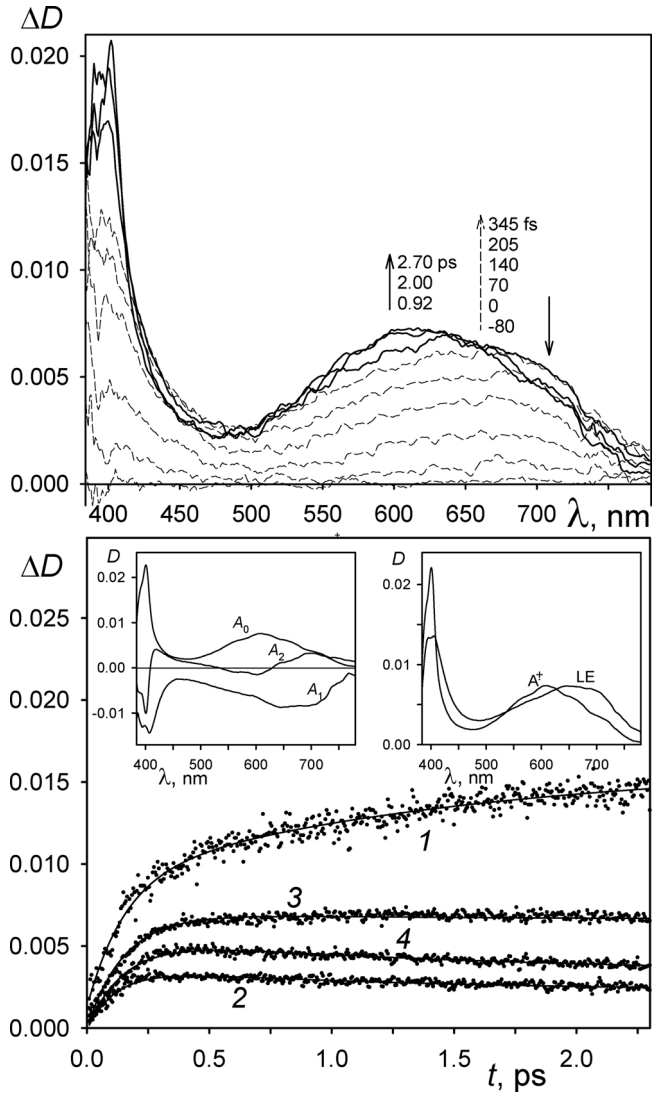

Fig. 5. *Above:* The dynamics of transient absorption spectra of **A** (C = 0.5 mM), which correspond to −80 to 345 fs delays (dash lines) and to 0.92 to 2.70 ps delays (solid lines), after the excitation by 260 nm 40 fs laser pulse. *Below:* The kinetic curves of transient absorption spectra for several wavelengths: (*1*) 400 nm, (*2*) 460 nm, (*3*) 650 nm, (*4*) 720 nm. The solid lines represent fitting by two-exponential function with characteristic times 140 fs and 1.95 ps. *Left Inset:* DAS correspond to characteristic times: (A_0) remaining spectrum, (A_1) 140 fs, (A_2) 1.95 ps. *Right Inset:* Absorption spectra of locally excited (LE) state of **A** and its cation-radical ($\mathbf{A}^{\cdot+}$).

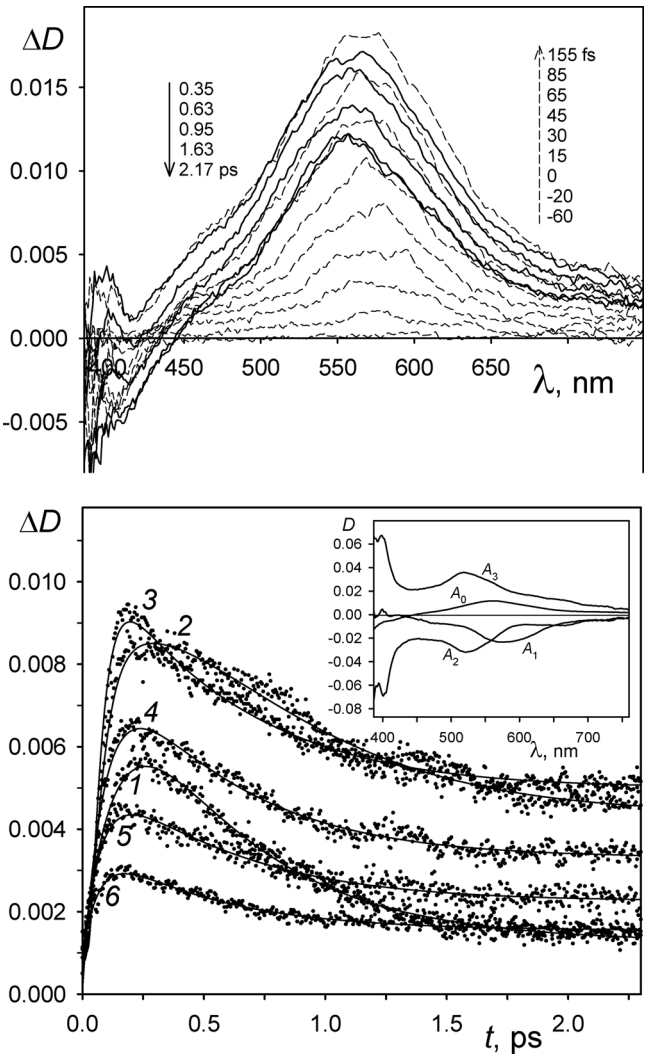

Fig. 6. *Above:* The dynamics of transient absorption spectra of **D**·**A** (C = 0.33 mM), which correspond to −60 to 155 fs delays (dash lines) and to 0.35 to 2.17 ps delays (solid lines), after the excitation by 330 nm 30 fs laser pulse. *Below:* The kinetic curves of transient absorption spectra for several wavelengths: (*1*) 460 nm, (*2*) 500 nm, (3) 600 nm (×0.5), (*4*) 660 nm, (*5*) 720 nm, (*6*) 780 nm. The solid lines represent fitting by three-exponential function with characteristic times 50 fs, 270 fs and 400 fs. *Inset:* DAS correspond to characteristic times: (A_0) remaining spectrum, (A_1) 50 fs, (A_2) 270 fs, (A_3) 400 fs.

emission (Fig. 4, *Above*) takes place due to the contribution of rising component **Ia**. Then, the spectral intensity and shape remain unchanged during next dozens of picoseconds after excitation. Remaining spectrum review in a wider time scale (500 ps) shows its slow mono-exponential decay with the characteristic time 640 ps (Fig. 4, *Above*). The DAS have the following physical meaning: A_1 with 557 nm maximum in absolute value (Table 2) approximately corresponds to inverted $S_1 \rightarrow S_n$ spectrum of S_1 state of **D**, while remaining spectrum A_0 with 559 nm maximum corresponds to the direct spectrum of the same state. The found characteristic time of absorption growth (60 fs) is significantly higher than that of excitation pulse front growth (10 fs). That is why, the presence of the component **Ia** cannot be explained by the finite duration of the excitation pulse. It can be referred to as the relaxation of Franck-Condon S_1 excited state.

Fig. 5 (*Above*) shows the dynamics of transient absorption spectra of **A** (C = 0.5 mM) during the first 3 ps after the excitation by 260 nm 40 fs laser pulse. Spectral changes are satisfactory described by Eq. (5) with two exponents and characteristic times 140 fs (**IIa**) and 1950 fs (**IIb**) (Fig. 5, *Below*). The *Left Inset* to Fig. 5 shows the spectral contributions of the components **IIa** (A_1), **IIb** (A_2) and remaining spectrum (A_0). During the first 400 fs, the growth of differential absorption takes place at 660 nm (Fig. 5, *Above*) due to the contribution of rising component **IIa**. During next 5 ps, a relatively slow shift of absorption maximum towards 600 nm is observed due to the contribution of rising component **IIb**. Then the spectral intensity and shape remained unchanged during next several picoseconds. Remaining spectrum review in a wider time scale (500 ps) shows its mono-exponential decay with the characteristic time 58 ps. The component **IIb** was referred to as the reduction of locally excited (LE) state **A*** into cation-radical $\mathbf{A}^{\cdot+}$ by capturing an electron from solvent molecule or from counterion, because its absorption maxima (401 nm and 602 nm) (Table 2) turned out to be close to those of the monomer of methylviologen cation-radical (396 nm and 602 nm in DMFA) [35]. The DAS have the following physical meaning: A_1 with 407 nm and 648 nm maxima (Table 2) approximately

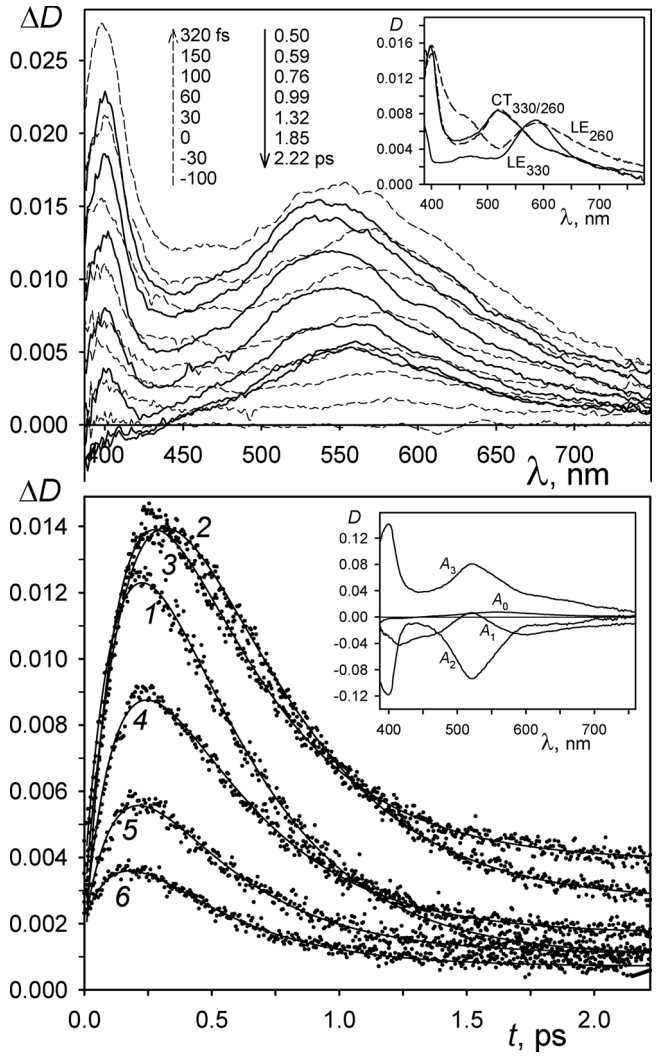

Fig. 7. *Above:* The dynamics of transient absorption spectra of **D·A** (C = 0.5 mM), which correspond to −100 to 320 fs delays (dash lines) and to 0.50 to 2.22 ps delays (solid lines), after the excitation by 260 nm 40 fs laser pulse. *Inset Above:* Absorption Spectra of LE and CT states, obtained by excitation at 260 nm (LE_{260} and CT_{260}) and 330 nm (LE_{330} and CT_{330}) laser pulse. *Below:* The kinetic curves of transient absorption spectra for several wavelengths: (*1*) 470 nm, (*2*) 500 nm, (*3*) 600 nm, (*4*) 660 nm, (*5*) 720 nm, (*6*) 780 nm. The solid lines represent fitting by three-exponential function with characteristic times 140 fs, 250 fs and 400 fs. *Inset Below:* DAS correspond to characteristic times: (A_0) remaining spectrum, (A_1) 140 fs, (A_2) 250 fs, (A_3) 400 fs.

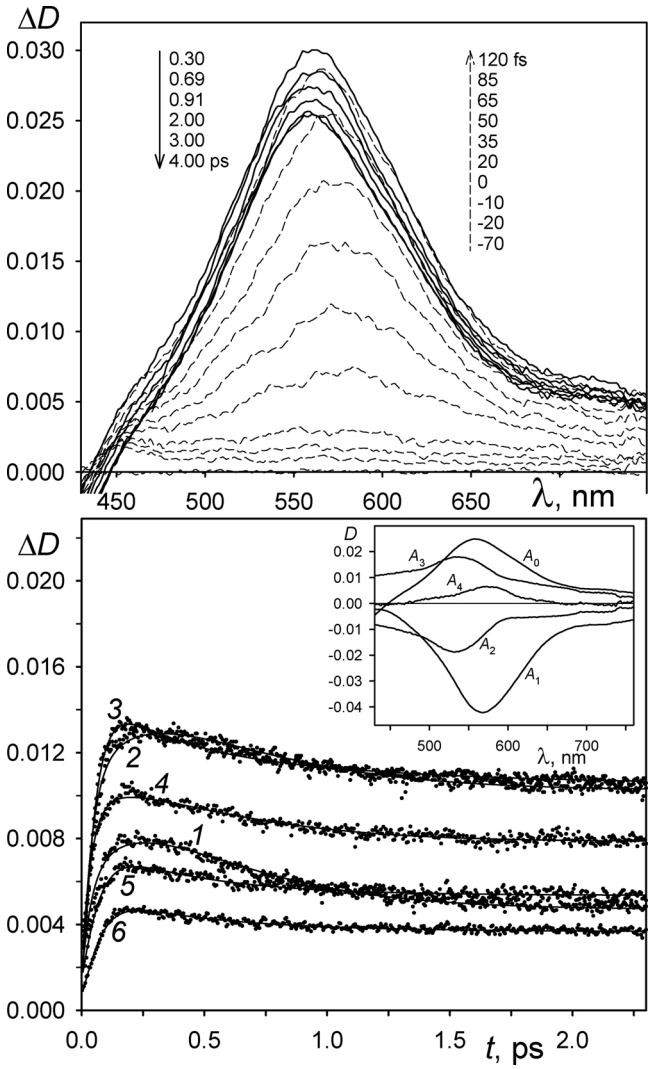

Fig. 8. *Above:* The dynamics of transient absorption spectra of 3:1 mixture of **D** (C = 2.0 mM) and **A** (C = 0.66 mM), which correspond to −70 to 120 fs delays (dash lines) and to 0.30 to 4.00 ps delays (solid lines), after the excitation by 30 fs 330 nm laser pulse. *Below:* The kinetic curves of transient absorption spectra for several wavelengths: (*1*) 470 nm, (*2*) 500 nm, (*3*) 600 nm (×0.5), (*4*) 660 nm, (*5*) 720 nm, (*6*) 780 nm. The solid lines represent fitting by four-exponential function with characteristic times 50 fs, 270 fs, 390 fs and 770 fs. *Inset:* DAS correspond to characteristic times: (A_0) remaining spectrum, (A_1) 50 fs, (A_2) 270 fs, (A_3) 390 fs, (A_4) 770 fs.

corresponds to the inverted spectrum of LE state of **A**. Spectrum A_2 with 401 nm and 602 nm maxima corresponds to a linear combination of absorption spectra of LE state and cation-radical $\mathbf{A}^{\cdot+}$. Remaining spectrum A_0 with 401 nm and 610 nm maxima corresponds to the absorption spectrum of cation-radical $\mathbf{A}^{\cdot+}$. The *Right Inset* to Fig. 5 shows absorption spectra of locally excited (LE) state of **A** and its cation-radical ($\mathbf{A}^{\cdot+}$).

Fig. 6 (*Above*) shows the dynamics of transient absorption spectra of **D·A** (C = 0.33 mM) after the pumping by 330 nm 30 fs laser pulse. The evolution of spectra is satisfactorily described by Eq. (5) for three exponents with characteristic times 50 fs (**IIIa**), 270 fs (**IIIb**) and 400 fs (**IIIc**) (Fig. 6, *Below*). The spectral contributions of each exponent are shown in the *Inset* (Fig. 6). During the first 200 fs after the pumping, a rise of transient absorption (Fig. 6, *Above*) takes place due to the component **IIIa** (A_1) with 574 nm maximum (Fig. 6, *Inset*). This process was referred to as the relaxation of LE state. During the period between 200 fs and 400 fs, a blue shift of spectra take place due to the rising component **IIIb** (A_2) with 400 nm and 522 nm maxima. This process was referred to as the conversion of the LE state into the CT state. Then, during the last 2 ps, a decay of transient absorption to the remaining level takes place due to the component **IIIc** (A_3) with 399 nm and 523 nm maxima. This process was referred to as the conversion of the CT state into the ground state. By physical meaning, spectrum A_1 corresponds to a linear combination of non-relaxed and relaxed LE state spectra, A_2 corresponds to a linear combination of LE and CT state spectra with predominant contribution of inverted CT state spectrum, A_3 is an absorption spectrum of CT state, remaining spectrum A_0 with 559 nm maximum is $S_1 \rightarrow S_N$ spectrum of **D**, which is formed as a result of equilibrium dissociation of **D·A**. Since CT state of **D·A** is of biradical nature and can be written as $\mathbf{D}^{\cdot+}\mathbf{A}^{\cdot+}$, it makes sense to compare the CT state absorption maximum with those for $\mathbf{D}^{\cdot+}$ and $\mathbf{A}^{\cdot+}$ cation-radicals. The found value (523 nm) is in a good agreement with that of 4,4′-dimethoxystilbene cation-radical (530 nm in MeCN) [36] and dimer of

methylviologen cation-radical (527 nm in water) [35].

In order to study the effects of excitation wave-length on the dynamics of excited **D·A** states and to check the possibility of CT state formation upon selective excitation of acceptor subsystem, we analyzed transient absorption spectra upon the excitation by 260 nm laser pulse (Fig. 7, *Above*). An increase in **D·A** concentration as compared with that used 330 nm excitation for femtosecond kinetics is connected with a lesser optic density of **D·A** at 260 nm wavelength (Fig. 1). As in the previous case, the dynamics of transient absorption spectra is satisfactorily described by three exponents and generally corresponds to that upon excitation by 330 nm laser pulse, when selective donor subsystem excitation takes place. The *Inset* to Fig. 7 (*Below*) shows spectral contributions of characteristic times 140 fs (**IVa**), 250 fs (**IVb**), and 400 fs (**IVc**). As follows from Table 2, a change of excitation light wavelength from 330 nm to 260 nm leads to an increase in characteristic time of the shortest component from 50 fs to 140 fs, as well as to a shift of vector maximum from 574 nm to 601 nm. This indicates that 260 nm initial local excitation is localized on the acceptor molecule, while 330 nm initial local excitation is localized on the donor molecule. At the same time, the position of CT state maximum (523 nm) remained unchanged. The times of formation and decay of CT states are approximately equal to the times upon 330 nm excitation. This is consistent with data obtained earlier for **D·A2** and **D·A3**, where the time of back electron transfer did not depend on the wave-length of excitation light [17,22]. A lower level of remaining spectrum in Fig. 7 as compared to Fig. 6 is explained by a small absorption of **D** at 260 nm.

In order to study the dynamics of **D·A·D** excited states, we obtained the transient absorption spectra of the solution, which contained a triple excess of **D** in relation to **A** (Fig. 8, *Above*). The equilibrium donor distribution under these conditions is described as follows: 54% of donor molecules are present as **D**, 21% as **D·A**, 25% as **D·A·D**. Comparison Figs. 8 with 7 and 6 shows that, under the conditions of **D** excess, the decay of transient absorption spectra down to remaining level takes approximately 3 ps instead 2 ps. This indicates the presence of an additional picosecond component in the spectra of Fig. 8, which is absent in other cases. SVD decomposition of optical density matrices, shown in Figs. 8 and 6, indicates an approximate equality of the fifth normalized diagonal element of the first matrix and the fourth normalized diagonal element of the second matrix. This suggests that the number of absorbing components in the first case is greater than in the second case. According to this, four exponents are required for satisfactory description of the dynamics of **D·A·D** transient absorption spectra. Fig. 8 (*Inset*) shows spectral contributions of characteristic times 50 fs (**Va**), 270 fs (**Vb**), 390 fs (**Vc**) and 770 fs (**Vd**). Comparison of spectral-kinetic characteristics of **Va**, **Vb** and **Vc** with those of **IIIa**, **IIIb** and **IIIc** (Table 2) shows generally their equality within 2–3%, that is why the greatest interest is **Vd** with a 770 fs decay time. It was referred to as **D·A·D** CT state lifetime, and the corresponding spectrum A_4 (Fig. 8, *Inset*) was referred to as **D·A·D** CT state absorption spectrum.

The time of back electron transfer in **D·A** (400 fs) is close to analogous time, obtained earlier for **D·A2** (410 fs). However, changes in free Gibbs energy, found from electrochemical data [21], are significantly different and equal to -1.46 eV and -1.67 eV, respectively (Table 3). Similarly, the characteristic time of back electron transfer for **D·A3** (540 fs) [17] is close to that of **D·A1** (510 fs), which is formed between **D** and 1,1′-bis(2-ammoniopropyl)-4,4′-bipyridinium tetraperchlorate (**A1**) [37]. Thus, in a number of 1:1 donor-acceptor complexes, formed by derivatives of 4,4′-bipyridinium and di-(4-pyridinium)-ethylene with ammonioethyl and ammoniopropyl *N*-substituents, the rate of back electron transfer depends weakly on the acceptor nature, but is determined by the length of the carbon chain of terminal groups. The independence of recombination rate of ion-radical pairs of reaction driving force within the range 0.4–2.0 eV was observed in work [38].

For revealing of the physical sense of pre-exponential factor vectors $A_i(\lambda)$ in Eq. (5) we suggested the following scheme of subsequent transformations:

$$LE^* \xrightarrow{k_1} LE \xrightarrow{k_2} CT \xrightarrow{k_3} GS \tag{6}$$

Here, LE* is an initial local excited state, LE is a relaxed local excited state, CT is a charge transfer state, GS is a ground state, k_1, k_2, k_3 are reaction rate constants. Then the dependence of concentrations of intermediate particles on time t in case of instant excitation up to the initial concentration C_0 can be written as:

$$[LE^*] = C_0 e^{-k_1 t} \tag{7}$$

$$[LE] = C_0 \frac{k_1}{k_1 - k_2}(e^{-k_2 t} - e^{-k_1 t}) \tag{8}$$

$$[CT] = C_0 \frac{k_1 k_2}{(k_1 - k_2)(k_1 - k_3)(k_2 - k_3)} \cdots$$
$$\cdots \{(k_1 - k_2)e^{-k_3 t} - (k_1 - k_3)e^{-k_2 t} + (k_2 - k_3)e^{-k_1 t}\} \tag{9}$$

By comparing Eq. (5) with Eqs. (7)–(9), using Beer-Lambert law and assuming $k_1 > > k_2 > k_3$, $C_0 = 1$, for a given wavelength we obtain:

$$A_1 = \varepsilon_{LE*} - \frac{k_1}{k_1 - k_2}\varepsilon_{LE} + \frac{k_1 k_2}{(k_1 - k_2)(k_1 - k_3)}\varepsilon_{CT} \approx -\varepsilon_{LE} \tag{10}$$

$$A_2 = \frac{k_1}{k_1 - k_2}\varepsilon_{LE} - \frac{k_1 k_2}{(k_1 - k_2)(k_2 - k_3)}\varepsilon_{CT} \approx \varepsilon_{LE} - \frac{k_2}{k_2 - k_3}\varepsilon_{CT} \tag{11}$$

$$A_3 = \frac{k_1 k_2}{(k_1 - k_3)(k_2 - k_3)}\varepsilon_{CT} \approx \frac{k_2}{k_2 - k_3}\varepsilon_{CT} \tag{12}$$

In Eqs. (10)–(12), ε_{LE} and ε_{CT} are molar absorption coefficients for LE and CT states, $\varepsilon_{LE^*} \approx 0$, because at the initial moment of time the absorption is small. As is seen from Eqs. (10)–(12), for the case $k_1 > > k_2 > k_3$, the vector $A_1(\lambda)$ is approximately an inverted absorption spectrum of LE state; the vector $A_2(\lambda)$ is a linear combination of absorption spectra of LE and CT states with dominant negative contribution of CT state spectrum; the vector $A_3(\lambda)$ is an absorption spectrum of CT state. In *Inset* to Fig. 7 (*Above)* the absorption spectra of LE and CT states are shown. Pairs of spectra were obtained upon excitation by a laser pulse with 330 nm and 260 nm wavelength. The absorption spectra of LE and CT states were recovered from DAS by means of their transformation according to Eqs. (11)–(12). Despite the differences in the shape of the spectrum fronts, the closeness of their maxima, their intensities and lifetimes indicates that relaxed LE and CT states are of the same nature irrespective of exciting light wavelength.

Table 3
Characteristic time of back electron transfer τ_{ET}, maximum position ν_{max}, bandwidth at half height $\Delta\nu_{1/2}$ and intensity ε_{max} of CT-band, matrix element H_{RP}, change of Gibbs free energy ΔG_0, high-frequency λ_2 reorganization energy for **D·A** and its analogues.

	τ_{ET}, fs	ν_{max}, cm^{-1}	$\Delta\nu_{1/2}$, cm^{-1}	ε_{max}, $M^{-1}\,cm^{-1}$	H_{RP}, eV	ΔG_0, eV	λ_2, eV
D·A	400	18900	6680	160	0.107	−1.46	0.12
D·A·D	770	16700	6200	720	0.205	−1.43	0.11
D·A1	510 [37]	20300	6280	210	0.102	−1.57	0.13
D·A2	410 [22]	18500	4880	331	0.130	−1.67	0.45
D·A3	540 [17]	19700	4880	375	0.103	−1.67	0.35
D·A3·D	1080 [17]	19200	5630	1020	0.180	−1.58	0.10

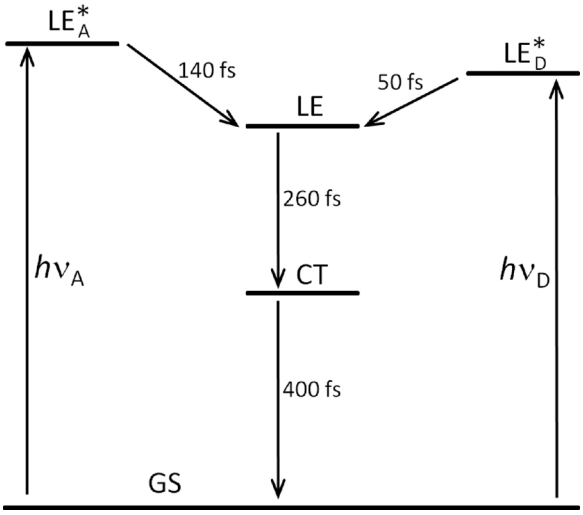

Scheme 1. Processes upon the excitation of **D·A** at 260 nm ($h\nu_A$) and at 330 nm ($h\nu_D$).

The wavelength of exciting light affects only LE state relaxation time. The given conclusion is shown graphically on Scheme 1:

Since the molar absorption of **D·A·D** is approximately five times higher than that for **D·A** (Table 1), according to Marcus theory, we could expect a significant increase in reaction rate of electron transfer when going from **D·A** to **D·A·D**. In practice, in the given case we observe two-times decrease of the reaction rate constant. In order to quantitatively take into account the effect of CTC structure on the electron transfer rate, we used the semiclassical single-mode nonadiabatic theory [25,39], which was enhanced by Barbara by including the solvent coordinate [40].

According to the theory, the rate of electron transfer in organic CTCs can be described as follows:

$$k_{ET}(t) = H_{RP}^2\left(\frac{4\pi^3}{h^2\lambda_1 kT}\right)^{1/2}\sum_{n=0}^{\infty}\frac{S^n}{n!}\exp\left[-S - \frac{(\Delta G_0+\lambda_1+\lambda_S[1-\exp(-t/\tau_S)]+nh\nu_a)^2}{4\lambda_1 kT}\right],$$
$$S = \frac{\lambda_2}{h\nu_a} \quad (13)$$

Here, $k_{ET}(t)$ is a time-dependent electron-transfer rate constant, H_{RP} is an electronic coupling matrix element, ΔG_0 is a change of Gibbs free energy, λ_1 and λ_2 are energies of reorganization, associated with low-frequency internal modes and with the averaged frequency ν_a of high-frequency internal modes, λ_S and τ_S are an energy and a time of solvent relaxation, respectively. When observed averaged time of electron transfer τ_{ET} can be calculated as follows:

$$\tau_{ET} = \int_0^{\infty} tQ(t)dt \Big/ \int_0^{\infty} Q(t)dt,$$
$$Q(t) = \exp\left[-\int_0^t k_{ET}(t)dt\right] \quad (14)$$

We used the following assumptions for comparing the experimental characteristic times of back electron transfer with the calculated values predicted from Eq. (14). Estimation of the matrix element H_{PR} was performed by Hush formula [40]:

$$H_{RP} = \frac{0.0206}{r}\sqrt{\nu_{max}\Delta\nu_{1/2}\varepsilon_{max}} \quad (15)$$

Here, ν_{max}, $\Delta\nu_{1/2}$ and ε_{max} are the parameters of Gaussian, which approximates the CT-band in the absorption spectrum of the complexes, r is an averaged distance between donor and acceptor planes. The values of r were taken from X-ray data and were fixed at 3.4 Å for **D·A**, **D·A·D** and **D·A2** [21], at 4.1 Å for **D·A1** [21], and for 4.7 Å for **D·A3** and **D·A3·D** [19]. The value of ΔG_0 was found from electrochemical data [21] as a difference between the reduction potential of the acceptor and the oxidation potential of the donor as components of a complex. Electrochemical potentials of 2:1 complexes were estimated as mean value of those for 1:1 complexes and for individual compounds, which leads to decreasing of the $-\Delta G_0$ values [17]. As in the work [30], the value of ν_a was equal to 1400 cm^{-1}. The internal temperature of the CT-state T was fixed at 300 K, assuming it to be close to room temperature [17]. The time of longitudinal relaxation τ_S of acetonitrile was assumed as 180 fs [17]. The reorganization energy λ_1 was fixed at 0.15 eV [17]. The reorganization energy λ_2 was an optimizable parameter. The reorganization energy λ_S was calculated from the complete reorganization energy λ_0 according to Eq. (16):

$$\lambda_0 = \lambda_1 + \lambda_2 + \lambda_S = \Delta G_0 + h\nu_{max} \quad (16)$$

Table 3 represents the values which were used for calculating the rates of back electron transfer according to Eq. (14) for **D·A** and its analogues. As is seen from the table, the 4,4′-bipyridinium derivatives have lower values of λ_2 reorganization energy than the derivatives of di-(4-pyridinium)-ethylene, which compensates a tendency to reaction rate growth due to a decrease in $-\Delta G_0$ value in inverse mode. In addition, the 2:1 complexes **D·A·D** and **D·A3·D** are characterized by a lower value of λ_2 reorganization energy compared with 1:1 complexes. In work [17] this fact is explained by the electron delocalization between two donor moieties in CT state of a 2:1 complex, which is confirmed by Raman spectroscopy [41]. As is shown from Table 3, the values of λ_2 reorganization energy of complexes **D·A·D** and **D·A3·D** are approximately the same, whereas **D·A** reorganization energy is twice as low as that for **D·A3**. This may be explained by non-planar geometry of **A** and steric disturbances in **D·A**, which manifests itself in its significant lesser stability and very small molar absorption coefficient.

3. Experimental

(*E*)-Bis(18-crown-6)stilbene (**D**) was prepared according to the work [42]. The synthesis of 1,1′-bis(2-ammonioethyl)-4,4′-bipyridinium tetraperchlorate (**A**) was carried out as described previously [21]. 1,8-Octanediammonium diperchlorate (**C8**), 1,10-decanediammonium diperchlorate (**C10**) and 1,12-dodecanediammonium diperchlorate (**C12**) were prepared from appropriate diamines and 70% perchloric acid (Aldrich) according to the work [43].

Anhydrous acetonitrile (Cryochrome, spectral grade, the water content < 0.03%) was used. Solutions were prepared in the light of red lamp to prevent *E–Z*-photoisomerization of the compounds **D**.

Steady-state absorption spectra were recorded on Shimadzu-3100 spectrophotometer. Steady-state fluorescence spectra were recorded on Perkin-Elmer LS-55 spectrofluorimeter. Fluorescence quantum yields were determined in aerated solutions relative to a solution of quinine bisulfate in 1*N* H_2SO_4 (ϕ = 0.546) used as a standard [44].

Transient absorption spectra were measured using a femtosecond pump–supercontinuum probe setup. The output of a "Tsunami" Ti/sapphire oscillator (800 nm, 80 MHz, 80 fs, Spectra-Physics, USA) was amplified by a "Spitfire" regenerative amplifier system (Spectra-Physics) at repetition rate 1 kHz. The amplified pulses were split into two beams. One of the beams was directed into a non-collinear phase-matched optical amplifier. A pair of quartz prisms compressed its output, which was centered at 740 nm. The second harmonics was used as a pump pulse. The Gauss pulse of 30 fs at 330 nm or 40 fs at 260 nm was tuned of the pump. The second beam was focused onto a thin quartz cell with H_2O to generate super-continuum probe pulses. The probe pulses were time-delayed with respect to each other. The pulses were then attenuated, recombined, and focused onto the sample cell. The pump and probe light spots had diameters of 300 and 120 μm, respectively. The pump pulse energy was attenuated to 50 nJ to optimize light excitation. All experiments were carried out at 295 K. Laser pulse frequency was adjusted by a SDG II Spitfire 9132 control amplifier (Spectra-Physics).

The pulse operation frequency was 50 Hz. The circulation rate in the flow cell of 0.5 mm thickness was adjusted to avoid multiple excitation. The relative polarization of pump and probe beams was adjusted to 54.7° (magic angle) in parallel and perpendicular polarizations. The super continuum signal out of the sample was dispersed by an Acton SP-300 polychromator and detected by a CCD camera (Roper Scientific SPEC-10). A time correction was applied at each kinetic trace. Control experiments were carried out for non-resonant signals from the pure solvent.

Transient Absorption Spectra were registered in 390–780 nm spectral range with a step of 1 nm and in 0–500 ps delay range with a varied step. A matrix of differential optic densities from 20 fs to 5 ps with a step of 5 fs was used for finding characteristic times of fast processes. The matrix from 20 fs to 10 ps was used for finding the time of the longer process of cation-radical $\mathbf{A}^{\cdot+}$ formation (2 ps). A matrix of differential optic densities from 5 ps to 500 ps with a step of 1 ps was used for finding characteristic times of slow processes. It should be noted that the lifetime of S_1 state of **D** is too great for its accurate determination on our installation. The intensity of S_1 state absorption is still great and is about half of the initial value after the lapse of 500 ps.

Non-linear optimization of constants was performed iteratively and consisted in minimization of functional F with the second order optimization function and Hessian numerical approximation [45]:

$$F(K, k) = \sum_{i,j} [D_{ij}^{e} - D_{ij}(K, k)]^2 \quad (17)$$

Here, $\boldsymbol{D}^{e}$ is an experimental matrix of optical densities, $\boldsymbol{D}(K,k)$ is a calculated matrix of optical densities, which depends on equilibrium (K) or kinetic (k) constants. Regarding to transient absorption spectra processing, the matrix of optical densities was calculated according to the formula:

$$\boldsymbol{D}(k) = \boldsymbol{AE}(k) \quad (18)$$

Here, $\boldsymbol{E}(k)$ is a matrix of decaying exponents of multi-exponential function (5) with an addition of unitary column for describing of a background or a remaining spectral component; $\boldsymbol{A}$ is a matrix of Decay Associated Spectra, which was estimated at every iteration of optimization according to formula [17]:

$$\boldsymbol{A} = \boldsymbol{D}^{e}\boldsymbol{E}^{T}(\boldsymbol{E}\boldsymbol{E}^{T})^{-1} \quad (19)$$

Relative errors for the values of equilibrium constants are estimated as 20%, of fluorescence quantum yields as 10%, and of characteristic times of transient absorption dynamics as 10%.

4. Conclusions

The spectral and thermodynamic properties of charge transfer complexes **D·A** and **D·A·D** between (*E*)-bis(18-crown-6)stilbene (**D**) and 1,1′-bis(2-ammonioethyl)-4,4′-bipyridinium tetraperchlorate (**A**) in MeCN were studied. **D·A** is highly stable, while **D·A·D** is weakly stable. Due to less steric hindrance, CT state absorption band of **D·A·D** is characterized by greater intensity and is shifted to a low-frequency area as compared to **D·A**.

D·A does not fluoresce due to fast intramolecular processes of direct and reverse electron transfer. The efficiency of **D·A** fluorescence ignition upon adding alkanediammonium salts depends on the length of a carbon chain. Supramolecular complex **D·A** can be regarded as a possible optic molecular sensor for determination of diammonium ions.

The spectral and kinetic characteristics of **D·A** and **D·A·D** CT states were obtained by femtosecond transient absorption spectroscopy. It was established that the characteristic time of back electron transfer in the CT state of **D·A·D** (770 fs) is significantly higher than that in the CT state of **D·A** (400 fs). This fact is explained by the electron delocalization between two donor moieties in **D·A·D**. A change of the wave-length of exciting light, leading to the displacement of excitation localization from donor to acceptor, within accuracy of the experiment, does not affect the rates of direct and back electron transfer, as well as the position of absorption maximum of CT state.

In a number of charge transfer complexes, formed by derivatives of 4,4′-bipyridinium and di-(4-pyridinium)-ethylene with ammonioethyl and ammoniopropyl *N*-substituents, the rate of back electron transfer depends weakly on the acceptor nature, but is determined by the length of the carbon chain of terminal groups.

Acknowledgements

This work was supported by the Russian Science Foundation (in respect of organic synthesis, grant number 14-13-00076); the Russian Foundation for Basic Research (grant number 17-03-00595); and the State Grant for the Semenov Institute of Chemical Physics, Russian Academy of Sciences (in respect of the femtosecond pumping and probe installation, grant number 0082-2018-0005, AAAA-A18-118020690203-8).

References

[1] R.O. Ebewele, Polymer Science and Technology, CRC Press, 2000.
[2] S.P. Panchenko, A.D. Averin, M.V. Anokhin, O.A. Maloshitskaya, I.P. Beletskaya, Cu (I)-catalyzed *N,N′*-diarylation of natural diamines and polyamines with aryl iodides, Beilstein J. Org. Chem. 11 (2015) 2297–2305.
[3] A. Späth, B. König, Molecular recognition of organic ammonium ions in solution using synthetic receptors, Beilstein J. Org. Chem. 6 (2010) 1–111.
[4] K. Fuji, K. Tsubaki, K. Tanaka, N. Hayashi, T. Otsubo, T. Kinoshita, Visualization of molecular length of α,ω-diamines and temperature by a receptor based on phenolphthalein and crown ether, J. Am. Chem. Soc. 121 (1999) 3807–3808.
[5] K. Tsubaki, H. Tanaka, T. Furuta, T. Kinoshita, K. Fujia, Recognition of the chain length of α,ω-diamines by a *meso*-ternaphthalene derivative with two crown ethers, Tetrahedron Lett. 41 (2000) 6089–6093.
[6] S.K. Kim, M.Y. Bang, S.-H. Lee, K. Nakamura, S.-W. Cho, J. Yoon, New fluorescent chemosensors for cationic guests: 1,8-bis(azacrown)anthracenes, J. Incl. Phenom. Macrocycl. Chem. 43 (2002) 71–75.
[7] D. Garozzo, G. Gattuso, A. Notti, A. Pappalardo, S. Pappalardo, M.F. Parisi, M. Perez, I. Pisagatti, A calix[5]arene-based heterotetratopic host for molecular recognition of long-chain, ion-paired α,ω-alkanediyldiammonium salts, Angew. Chem. Int. Ed. 44 (2005) 4892–4896.
[8] M.V. Rekharsky, Y. Ho Ko, N. Selvapalam, K. Kim, Y. Inoue, Complexation thermodynamics of cucurbit[6]uril with aliphatic alcohols, amines, and diamines, Supramol. Chem. 19 (2007) 39–46.
[9] M. Sirish, V.A. Chertkov, H.J. Schneider, Porphyrin-based peptide receptors: syntheses and NMR analysis, Chem. Eur. J. 8 (2002) 1181–1188.
[10] X.-K. Qu, L.-Y. Zhu, L. Li, X.-L. Wei, F. Liu, D.-Z. Sun, Host–guest complexation of β-, γ-cyclodextrin with alkyl trimethyl ammonium bromides in aqueous solution, J. Solut. Chem. 36 (2007) 643–650.
[11] J.H. Jung, H.Y. Lee, S.H. Jung, S.J. Lee, Y. Sakata, T. Kaneda, A color version of the Hinsberg test: permethylated cyclodextrin and crown-appended azophenol for highly selective sensing of amines, Tetrahedron 64 (2008) 6705–6710.
[12] S.P. Gromov, E.N. Ushakov, A.I. Vedernikov, N.A. Lobova, M.V. Alfimov, Yu.A. Strelenko, J.K. Whitesell, M.A. Fox, A novel optical sensor for metal ions based on ground-state intermolecular charge-transfer complexation, Org. Lett. 1 (1999) 1697–1699.
[13] E.N. Ushakov, S.P. Gromov, A.I. Vedernikov, E.V. Malysheva, A.A. Botsmanova, M.V. Alfimov, B. Eliasson, U.G. Edlund, J.K. Whitesell, M.A. Fox, Self-organization of highly stable electron donor-acceptor complexes via host-guest interactions, J. Phys. Chem. A 106 (2002) 2020–2023.
[14] K.P. Butin, A.A. Moiseeva, S.P. Gromov, A.I. Vedernikov, A.A. Botsmanova, E.N. Ushakov, M.V. Alfimov, Prospects of electroanalytical investigations of supramolecular complexes of a bis-crown stilbene with viologen-like compounds bearing two ammonioalkyl groups, J. Electro-Anal. Chem. 547 (2003) 93–102.
[15] I.S. Alaverdian, A.V. Feofanov, S.P. Gromov, A.I. Vedernikov, N.A. Lobova, M.V. Alfimov, Structure of charge-transfer complexes formed by bis-crown stilbene and dipyridylethylene derivatives as probed by surface-enhanced Raman scattering spectroscopy, J. Phys. Chem. A 107 (2003) 9542–9546.
[16] Yu.S. Alaverdyan, A.V. Feofanov, S.P. Gromov, A.I. Vedernikov, N.A. Lobova, M.V. Alfimov, Spectroscopy of surface-enhanced Raman scattering of a complex with charge transfer between a bis-crown-containing stilbene and a bis-ammonium-alkyl derivative of dipyridylethylene, Opt. Spectrosc. 97 (2004) 560–566.
[17] E.N. Ushakov, V.A. Nadtochenko, S.P. Gromov, A.I. Vedernikov, N.A. Lobova, M.V. Alfimov, F.E. Gostev, A.N. Petrukhin, O.M. Sarkisov, Ultrafast excited state dynamics of the bi- and termolecular stilbene-viologen charge-transfer complexes assembled via host–guest interactions, Chem. Phys. 298 (2004) 251–261.
[18] S.P. Gromov, A.I. Vedernikov, E.N. Ushakov, N.A. Lobova, A.A. Botsmanova, L.G. Kuz'mina, A.V. Churakov, Yu.A. Strelenko, M.V. Alfimov, J.A.K. Howard, D. Johnels, U.G. Edlund, Novel supramolecular charge-transfer systems based on bis (18-crown-6)stilbene and viologen analogues bearing two ammonioalkyl groups,

New J. Chem. 29 (2005) 881–894.
[19] A.I. Vedernikov, L.G. Kuz'mina, N.A. Lobova, E.N. Ushakov, J.A.K. Howard, M.V. Alfimov, S.P. Gromov, Unusual three-decker structure of a D–A–D complex between bis(crown)stilbene and a di(quinolyl)ethylene derivative, Mendeleev Commun. 17 (2007) 151–153.
[20] S.P. Gromov, A.I. Vedernikov, E.N. Ushakov, M.V. Alfimov, Unusual supramolecular donor-acceptor complexes of bis(crown)stilbenes and bis(crown)azobenzene with viologen analogs, Russ. Chem. Bull. 57 (2008) 793–801.
[21] A.I. Vedernikov, E.N. Ushakov, A.A. Efremova, L.G. Kuz'mina, A.A. Moiseeva, N.A. Lobova, A.V. Churakov, Yu.A. Strelenko, M.V. Alfimov, J.A.K. Howard, S.P. Gromov, Synthesis, structure, and properties of supramolecular charge-transfer complexes between bis(18-crown-6)stilbene and ammonioalkyl derivatives of 4,4'-bipyridine and 2,7-diazapyrene, J. Org. Chem. 76 (2011) 6768–6779.
[22] M.V. Rusalov, V.V. Volchkov, V.L. Ivanov, M.Ya. Melnikov, I.V. Shelaev, F.E. Gostev, V.A. Nadtochenko, A.I. Vedernikov, S.P. Gromov, M.V. Alfimov, Femtosecond excited state dynamics of a stilbene-viologene charge transfer complex assembled via host-guest interactions, Photochem. Photobiol. Sci. 16 (2017) 1800–1811.
[23] V.V. Volchkov, M.V. Rusalov, F.E. Gostev, I.V. Shelaev, V.A. Nadtochenko, A.I. Vedernikov, A.A. Efremova, L.G. Kuz'mina, S.P. Gromov, M.V. Alfimov, M.Ya. Melnikov, Complexation of bis-crown stilbene with alkali and alkaline-earth metal cations. Ultrafast excited state dynamics of the stilbene-viologen analogue charge transfer complex, J. Phys. Org. Chem. 31 (2018) e3759.
[24] T. Kumpulainen, B. Lang, A. Rosspeintner, E. Vauthey, Ultrafast elementary photochemical processes of organic molecules in liquid solution, Chem. Rev. 117 (2017) 10826–10939.
[25] B.S. Brunschwig, N. Sutin, Rate-constant expressions for nonadiabatic electron-transfer reactions, Comments Inorg. Chem. 6 (1987) 209–235.
[26] N. Mataga, T. Asahi, Y. Kanda, T. Okada, T. Kakitani, The bell-shaped energy gap dependence of the charge recombination reaction of geminate radical ion pairs produced by fluorescence quenching reaction in acetonitrile solution, Chem. Phys. 127 (1988) 249–261.
[27] N. Mataga, H. Chosrowjan, Y. Shibata, N. Yoshida, A. Osuka, T. Kikuzawa, T. Okada, First unequivocal observation of the whole bell-shaped energy gap law in intramolecular charge separation from S_2 excited state of directly linked porphyrin-imide dyads and its solvent-polarity dependencies, J. Am. Chem. Soc. 123 (2001) 12422–12423.
[28] T. Asahi, N. Mataga, Y. Takahashi, T. Miyashi, Energy gap dependence of the charge recombination process of ion pairs produced by excitation of 2,6,9,10-tetracyanoanthracene – methylsubstituted benzene charge transfer complexes in acetonitrile, Chem. Phys. Lett. 171 (1990) 309–313.
[29] O. Nicolet, E. Vauthey, Ultrafast nonequilibrium charge recombination dynamics of excited donor-acceptor complexes, J. Phys. Chem. A 106 (2002) 5553–5562.
[30] W. Jarzęba, Sh. Murata, M. Tachiya, Ultrafast dynamics of the excited tetracyanoethylene–toluene electron donor–acceptor complex, Chem. Phys. Lett. 301 (1999) 347–355.
[31] T. Okada, M. Migita, N. Mataga, Y. Sakata, S. Misumi, Picosecond laser spectroscopy of intramolecular heteroexcimer systems. Time-resolved absorption studies of p-$(CH_3)_2NC_6H_4(CH_2)_n$(1-pyrenyl) and -(9-anthryl) systems, J. Am. Chem. Soc. 103 (1981) 4715–4720.
[32] A.M. Swinnen, M. Van der Auweraer, F.C. de Schryver, K. Makatani, T. Okada, N. Mataga, Photophysics of the intramolecular exciplex formation in ω-(1-pyrenyl)-α-*N,N*-dimethylaminoalkanes, J. Am. Chem. Soc. 109 (1987) 321–330.
[33] G. Duvanel, N. Banerji, E. Vauthey, Excited-state dynamics of donor-acceptor bridged systems containing a boron-dipyrromethene chromophore: interplay between charge separation and reorientational motion, J. Phys. Chem. A 111 (2007) 5361–5369.
[34] L. Sánchez, N. Martín, D.M. Guldi, Hydrogen-bonding motifs in fullerene chemistry, Angew. Chem. Int. Ed. 44 (2005) 5374–5382.
[35] Ch. Lee, Y.M. Lee, M.S. Moon, S.H. Park, J.W. Park, K.G. Kim, S.-J. Jeon, UV-vis-NIR and Raman spectroelectrochemical studies on viologen cation radicals: evidence for the presence of various types of aggregate species, J. Electroanal. Chem. 416 (1996) 139–144.
[36] E. Steckhan, Spectroelectrochemical studies of olefins. 3. The dimerization mechanism of the 4,4'-dimethoxystilbene cation radical in the absence and presence of methanol, J. Am. Chem. Soc. 100 (1978) 3526–3533.
[37] V.V. Volchkov, M.N. Khimich, M.V. Rusalov, F.E. Gostev, I.V. Shelaev, V.A. Nadtochenko, A.I. Vedernikov, S.P. Gromov, A.Ya. Freidzon, M.V. Alfimov, M.Ya. Melnikov, Formation of supramolecular charge-transfer complex. Ultrafast excited state dynamics and quantum-chemical calculations, Photochem. Photobiol. Sci. 18 (2019), https://doi.org/10.1039/C8PP00328A.
[38] W. Jarzęba, Ultrafast electron transfer in arene–Br atom charge transfer complexes, J. Mol. Liq. 68 (1996) 1–11.
[39] H. Sumi, R.A. Marcus, Dynamical effects in electron transfer reactions, J. Chem. Phys. 84 (1986) 4894–4914.
[40] P.F. Barbara, T.J. Meyer, M.A. Ratner, Contemporary issues in electron transfer research, J. Phys. Chem. 100 (1996) 13148–13168.
[41] B.M. Britt, J.L. McHale, Resonance Raman study of a two-chromophore system. The 2:1 complex of hexamethylbenzene with tetracyanoethylene, Chem. Phys. Lett. 270 (1997) 551–556.
[42] A.I. Vedernikov, S.S. Basok, S.P. Gromov, L.G. Kuz'mina, V.G. Avakyan, N.A. Lobova, E.Yu. Kulygina, T.V. Titkov, Yu.A. Strelenko, E.I. Ivanov, J.A.K. Howard, M.V. Alfimov, Synthesis and structure of bis-crown-containing stilbenes, Russ. J. Org. Chem. 41 (2005) 843–854.
[43] S.P. Gromov, A.I. Vedernikov, L.G. Kuz'mina, N.A. Lobova, S.S. Basok, Yu.A. Strelenko, M.V. Alfimov, Stereoselective [2 + 2] photocycloaddition in bispseudosandwich complexes of bis(18-crown-6) stilbene with alkanediammonium ions, Russ. Chem. Bull. 58 (2009) 108–114.
[44] W.H. Melhuish, Quantum efficiencies of fluorescence of organic substances – effect of solvent and concentration of fluorescence solute, J. Phys. Chem. 65 (1961) 229–235.
[45] M.V. Rusalov, Numerical simulation of chemical equilibria and photostationary states using spectrophotometric and spectrofluorometric data, Russ. J. Gen. Chem. 75 (2005) 351–358.